ChemComm

COMMUNICATION

View Article Online
View Journal | View Issue

Cite this: *Chem. Commun.*, 2023, **59**, 7947

Received 18th April 2023,
Accepted 26th May 2023

DOI: 10.1039/d3cc01902k

rsc.li/chemcomm

Optimizing $LiMn_{1.5}M_{0.5}O_4$ cathode materials for aqueous photo-rechargeable batteries†

Kohei Shimokawa, *[ab] Shogo Matsubara, [c] Tomoya Kawaguchi, [b] Akihiro Okamoto [defg] and Tetsu Ichitsubo *[bh]

Spinel oxides are promising for high-potential cathode materials of photo-rechargeable batteries. However, $LiMn_{1.5}M_{0.5}O_4$ (M = Mn) shows a rapid degradation during charge/discharge under the illumination of UV-visible light. Here, we investigate various spinel-oxide materials by modifying the composition (M = Fe, Co, Ni, Zn) to demonstrate photocharging in a water-in-salt aqueous electrolyte. $LiMn_{1.5}Fe_{0.5}O_4$ exhibited a substantially higher discharge capacity compared to that of $LiMn_2O_4$ after long-term photocharging owing to enhanced stability under illumination. This work provides fundamental design guidelines of spinel-oxide cathode materials for the development of photo-rechargeable batteries.

Energy harvesting and storage from renewable sources is one of the most important issues for achieving a sustainable society. Solar cells can supply electricity from sunlight; however, they must be connected to rechargeable batteries for storing energy. Photo-rechargeable batteries (PRBs),[1,2] which can generate and store electricity in one device, are promising to address this problem. Since the first report in 1976,[3] the development of PRBs has been limited by the lack of suitable electrode materials. Nevertheless, PRBs are now attracting much attention due to the growing demand for next-generation batteries. In addition, PRBs are expected to be used for internet of things (IoT) devices, where photocharging would significantly improve the utility of such wireless devices. Various configurations of PRBs have been proposed so far,[4–12] and they roughly fall into two types: three-[7–9] and two-electrode[4–6,10–12] systems. The two-electrode design is suitable for reducing the cost and size owing to the absence of an additional photoelectrode.[1,2] Furthermore, tailoring the electrode materials is important to improve the performance and the feasibility of practical applications.[13–16]

Our group recently reported the photocharging of $LiMn_2O_4$, in which we employed a half-cell with an electron acceptor to demonstrate Li extraction from the spinel structure induced by the holes generated in TiO_2 nanoparticles.[17] Spinel $LiMn_2O_4$ is promising for a high-potential cathode; however, a problem is its low stability during charge/discharge. For instance, it is well known that Mn^{2+} formed by the disproportionation of Mn^{3+} in $LiMn_2O_4$ easily dissolves into electrolytes,[18] resulting in capacity fading. The disproportionation is considered to be accelerated under illumination due to the photoexcitation of electrons in Mn d-orbitals.[19,20] Thus, the stability should be enhanced by materials design to improve the battery performance.

To investigate the stability of $LiMn_2O_4$ under illumination, we performed cyclic voltammetry (CV) in a water-in-salt LiTFSA (TFSA: bis(trifluoromethanesulfonyl)amide) solution, which is a highly-concentrated aqueous electrolyte[21] used in our previous work.[17] $LiMn_2O_4$ showed high cyclability in the dark;[17] however, as shown in Fig. 1, a rapid capacity fading was observed under the illumination of UV-visible light (300–600 nm; $\sim$0.36 W cm^{-2}) to the electrode. This indicates that the degradation of $LiMn_2O_4$ was significantly accelerated under illumination. A conventional way to improve the stability against disproportionation is substituting a part of the Mn in $LiMn_2O_4$ with other elements.[22–24] Considering that the disproportionation proceeds with multiple Mn^{3+} cations in the structure, decreasing the density of Mn^{3+} is effective for preventing it. The molar ratio of Mn^{3+}/Mn^{4+}, which is 1 for $LiMn_2O_4$, can be tuned by partially substituting Mn with other elements.

[a] *Frontier Research Institute for Interdisciplinary Sciences, Tohoku University, 6-3 Aramaki Aza Aoba, Aoba-ku, Sendai 980-8578, Japan. E-mail: kohei.shimokawa.b7@tohoku.ac.jp*
[b] *Institute for Materials Research, Tohoku University, 2-1-1 Katahira, Aoba-ku, Sendai 980-8577, Japan. E-mail: tichi@imr.tohoku.ac.jp*
[c] *Department of Life Science and Applied Chemistry, Graduate School of Engineering, Nagoya Institute of Technology, Gokiso-cho, Show-ku, Nagoya 466-8555, Japan*
[d] *International Center for Materials Nanoarchitectonics (WPI-MANA), National Institute for Materials Science, 1-1 Namiki, Tsukuba, Ibaraki 305-0044, Japan*
[e] *Research Center for Macromolecules and Biomaterials, National Institute for Materials Science, 1-1 Namiki, Tsukuba, 305-0044, Japan*
[f] *Graduate School of Chemical Sciences and Engineering, Hokkaido University, North 13 West 8, Kita-ku, Sapporo, Hokkaido 060-8628, Japan*
[g] *Graduate School of Science and Technology, University of Tsukuba, 1-1-1 Tennodai, Tsukuba, 305-8577, Japan*
[h] *Advanced Science Research Center, Japan Atomic Energy Agency, 2-4 Shirakata, Tokai-mura, Naka-gun, Ibaraki 319-1195, Japan*

† Electronic supplementary information (ESI) available. See DOI: https://doi.org/10.1039/d3cc01902k

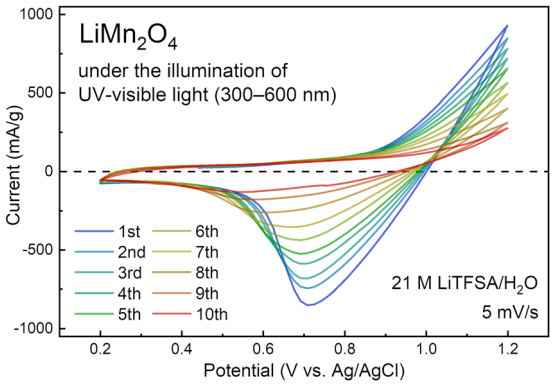

Fig. 1 CV profiles of $LiMn_2O_4$ under the illumination of UV-visible light (300–600 nm) in 21 M LiTFSA/H_2O.

In the case of $LiMn_{1.5}M_{0.5}O_4$, it becomes as follows: (i) when M is another trivalent cation (*e.g.*, Fe^{3+}, Co^{3+}), the Mn^{3+} density decreases to half ($Mn^{3+}/Mn^{4+} = 0.5$), (ii) when M is a divalent cation (*e.g.*, Ni^{2+}, Zn^{2+}), Mn^{3+} is ideally absent in the spinel structure ($Mn^{3+}/Mn^{4+} = 0$). However, a drawback is a decrease in the capacity due to the lowered number of Mn^{3+} cations,[25] which can be oxidized in charging. We, therefore, hypothesized that trivalent M is suitable for the $LiMn_{1.5}M_{0.5}O_4$ cathode of PRBs in terms of the balance of capacity and stability, as shown in Fig. 2(a).

We prepared four kinds of spinel-oxide cathode materials using Fe, Co, Ni, and Zn (Fig. 2(b)), based on previous works.[22–25] A solution combustion method was used for their synthesis.[26] The obtained materials were further calcined at 500 °C in an air atmosphere to remove the impurity phases and improve the crystallinity (Fig. S1–S5, ESI†). Their X-ray diffraction (XRD) profiles were analysed by the Rietveld method. The crystalline size was estimated to be ~10 nm for all the compositions (Fig. S6a, ESI†). $LiMn_{1.5}Fe_{0.5}O_4$ exhibited the largest lattice constant (Fig. S6b, ESI†), which is reasonable because Fe^{3+} in the high-spin state shows a large ionic radius in relation to the other substituting elements in the spinel structure.[27] Almost all Li ions were found to be located at the tetrahedral 8a site in the $Fd\bar{3}m$ space group (*i.e.*, normal spinel), except for $LiMn_{1.5}Zn_{0.5}O_4$ due to the strong preference of Zn for the tetrahedral site (Fig. S6c, ESI†).[27,28] This results in the enhanced intensity of the diffraction peak at ~31° for $LiMn_{1.5}Zn_{0.5}O_4$. Distributions of particle size were measured with a nanoparticle tracking analyser (NTA) as well as a scanning electron microscope (SEM), where the average values were approximately 200 nm (Fig. S7, ESI†). Furthermore, the compositions of the synthesized materials were confirmed by inductively coupled plasma optical emission spectroscopy (ICP-OES). The obtained molar ratios of Mn/M were almost the same as the nominal compositions (Table S1, ESI†).

Electrochemical activities of the synthesized materials were first evaluated by CV measurements in the dark condition. The water-in-salt electrolyte enables the charging/discharging of Mn-based spinel oxides due to its high oxidative stability.[17,21] Note that Mn-based spinel cathode materials exhibit multiple redox potentials,[18,25] *i.e.*, so-called 3, 4, and 5 V regions. Higher potential is better in terms of energy density; however, in this work, we focused on the 4 V region used for conventional Li-ion batteries considering the electrochemical stability window of the electrolyte.[21] We employed beaker-type and multichannel screen-printed electrode cells.[29] In both cases, redox reactions were clearly observed for $LiMn_{1.5}Fe_{0.5}O_4$ and $LiMn_{1.5}Co_{0.5}O_4$ (Fig. S8, ESI†). In contrast, only the capacitive current was observed for $LiMn_{1.5}Zn_{0.5}O_4$, which is consistent with previous literature.[25,30] $LiMn_{1.5}Ni_{0.5}O_4$ slightly showed redox capacities in the 4 V region, as also reported previously.[25,31] The above results indicate that the substituted Zn and Ni were almost divalent and therefore Mn^{3+} remained little in the spinel structure, which results in an increase in stability while a decrease in capacity.

Then we examined CVs using the beaker-type cells under illumination to the electrodes (Fig. S9, ESI†). As predicted in Fig. 2(a), $LiMn_{1.5}Ni_{0.5}O_4$ and $LiMn_{1.5}Zn_{0.5}O_4$ were highly stable even under the illumination of UV-visible light, while capacity fading was observed for the other compositions (Fig. S10, ESI†). A photoactive electrode can be prepared by mixing with TiO_2 nanoparticles,[17] and it is expected that the degradation of spinel materials is suppressed owing to the absorption of UV light by TiO_2. In fact, the cyclability under illumination was improved in the presence of TiO_2 (Fig. S11, ESI†), enabling us to use the target compositions such as $LiMn_{1.5}Fe_{0.5}O_4$ and $LiMn_{1.5}Co_{0.5}O_4$ in PRBs. On the other hand, a rapid decrease in the redox capacity was observed for $LiMn_2O_4$ even with TiO_2 (Fig. S12, ESI†), further supporting our concept. Although $LiMn_{1.5}Fe_{0.5}O_4$ still showed ~1% decrease in capacity for every cycle (Fig. S13, ESI†), it was also observed in the initial stage of conventional charge/discharge in the dark (Fig. S14, ESI†). Note that the current density jumped up when starting illumination, which can be attributed to a decrease in the charge-transfer resistance under UV-visible light illumination (Fig. S15, ESI†), as also previously reported.[11,12,19,20]

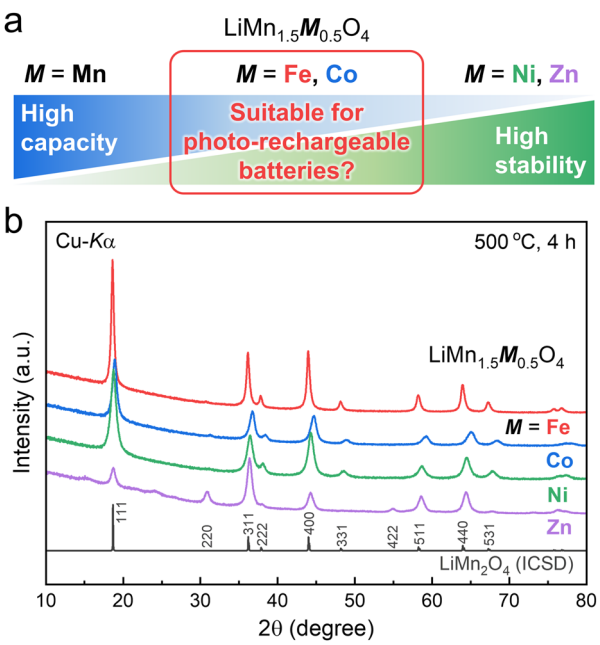

Fig. 2 (a) Overview of the materials design strategy in this study. (b) XRD profiles of the synthesized $LiMn_{1.5}M_{0.5}O_4$ (M = Fe, Co, Ni, Zn) after calcination at 500 °C for 4 h.

The photocharging performances of the cathode materials were evaluated by using a half-cell system with $K_2S_2O_8$ as an electron acceptor.[17] In this system, photoexcited electrons in TiO_2 (*ca.* −0.4 V *vs.* NHE) were consumed by the reduction of $S_2O_8^{2-}$, and the holes (*ca.* +2.8 V *vs.* NHE) drive Li extraction from the Mn-based spinel oxides (*ca.* +1 V *vs.* NHE).[17] The three-electrode beaker cell (Fig. S9, ESI†) used for the CV measurements was also employed for the photocharge/discharge experiments. $LiMn_{1.5}Fe_{0.5}O_4$ and $LiMn_{1.5}Co_{0.5}O_4$ were chosen as promising materials to further investigate the photocharging performance, together with $LiMn_{1.5}Zn_{0.5}O_4$ for comparison. $LiMn_{1.5}Ni_{0.5}O_4$ was not studied due to the little capacity in the 4 V region indicated in the aforementioned CV results. Note that the weight ratio of spinel oxide/TiO_2 was fixed to 1, and TiO_2 was homogeneously distributed in the electrodes (Fig. S16, ESI†). As shown in Fig. 3(a) and (b) (upper), a continuous increase in the open-circuit potential (OCP) under illumination was observed for $LiMn_{1.5}Fe_{0.5}O_4$ and $LiMn_{1.5}Co_{0.5}O_4$. In addition, the OCP became almost constant after turning the light off. However, it was not the case for $LiMn_{1.5}Zn_{0.5}O_4$; the potential increased by illumination, whereas it decreased after approximately 90 min and increased again after finishing the illumination for 120 min. Such unstable behaviour can be attributed to its little capacity. Indeed, the capacities in the subsequent discharging process were lower than 20 mA h g^{-1} (Fig. 3(c), lower). In contrast, $LiMn_{1.5}Fe_{0.5}O_4$ and $LiMn_{1.5}Co_{0.5}O_4$ showed substantial discharge capacities, which increased with increasing the photocharging time (Fig. 3(a) and (b), lower). The discharge capacities from around 1.0 V *vs.* Ag/AgCl clearly indicate the redox reactions of the Mn-based spinel-oxide cathode materials.[17] As demonstrated here, spinel oxides modified from $LiMn_2O_4$ were successfully photocharged, for what we believe is the first time.

The obtained discharge capacities are displayed in Fig. 4 for comparison with those of reported $LiMn_2O_4$.[17] In our previous work, we estimated the rate of photocharging in this system with TiO_2 and $K_2S_2O_8$, as shown by the grey line, where the slope (~23 mA g^{-1}) showed the photocharging rate based on ICP-OES.[17] However, the discharge capacities after photocharging $LiMn_2O_4$ were much lower than the expected values, especially for the long-term photocharging. This is probably due to the relatively low stability of $Li_xMn_2O_4$ under illumination (Fig. 1), leading to some amount of irreversible capacity. In contrast, the discharge capacities of $LiMn_{1.5}Fe_{0.5}O_4$ were in excellent agreement with those predicted by the grey line. In particular, they showed a linear relationship with the illumination time even for 120 min and were substantially higher than those for $LiMn_2O_4$. Since the theoretical capacity of $LiMn_{1.5}Fe_{0.5}O_4$ is supposed to be lower than that of $LiMn_2O_4$ (Fig. 2(a)), the improved discharge capacity is surely evidence of enhanced stability under illumination.

On the contrary, $LiMn_{1.5}Co_{0.5}O_4$ exhibited a lower discharge capacity compared to that of $LiMn_2O_4$ after photocharging for 120 min. Given the improved stability of $LiMn_{1.5}Co_{0.5}O_4$ under illumination (Fig. S11f, ESI†), there should be another factor for decreasing the efficiency of photocharging. Although this is still under investigation, a possible reason is the catalytic reaction of water oxidation; Co-based oxides are famous water oxidation catalysts,[32] and they tend to provide holes to water compared to Fe-based oxides as demonstrated in combination with TiO_2.[33]

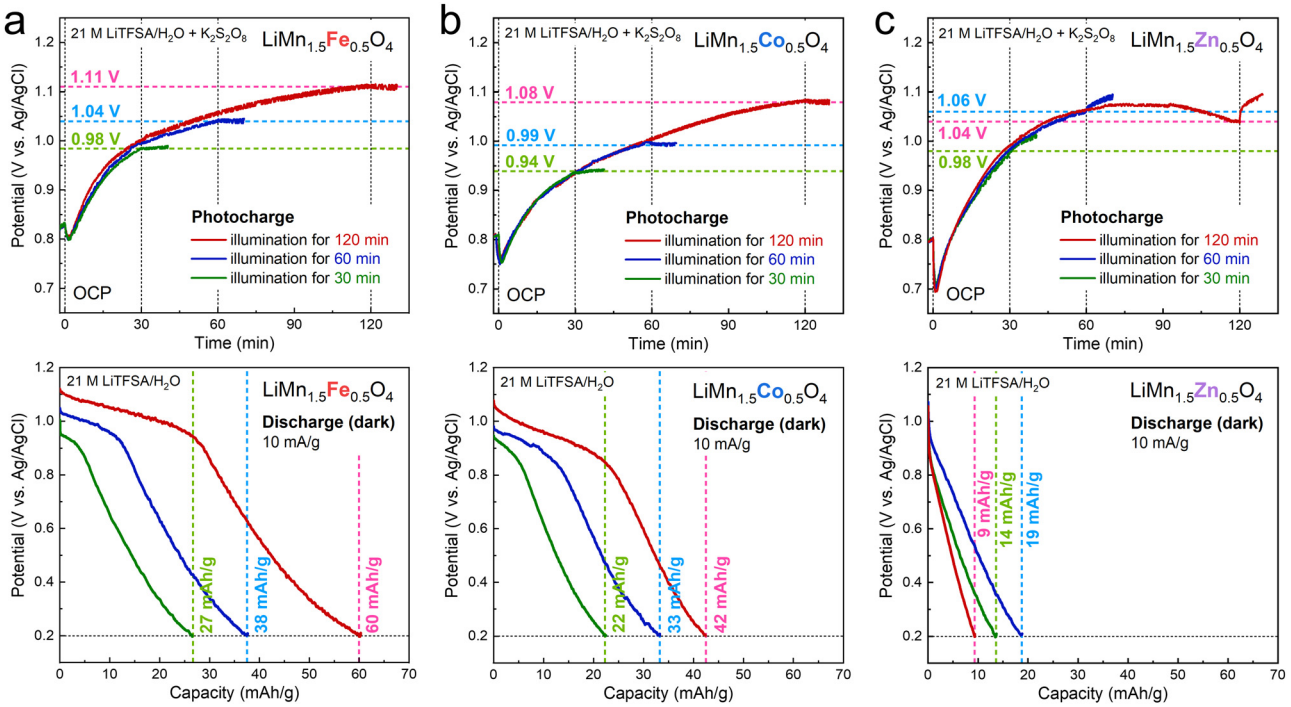

Fig. 3 (a)–(c) Open circuit potential (OCP) during the photocharging process under illumination in 21 M LiTFSA/H_2O with $K_2S_2O_8$ as an electron acceptor (upper) and discharging profiles in the dark condition for the electrodes after photocharging (lower), where the electrolyte used in the discharging process was 21 M LiTFSA/H_2O without $K_2S_2O_8$.

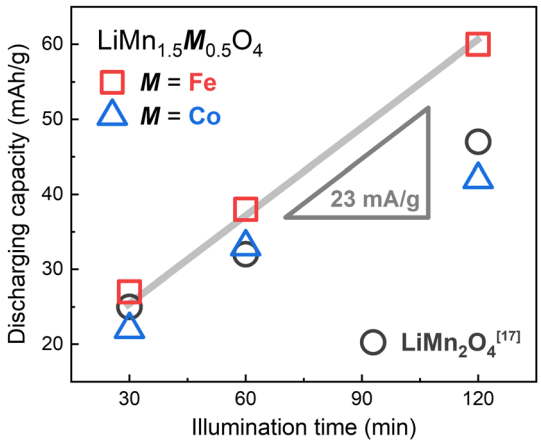

Fig. 4 Discharge capacities of $LiMn_{1.5}M_{0.5}O_4$ (M = Fe, Co) after the photocharging process together with our previous data for $LiMn_2O_4$.[17] The grey line indicates the previously estimated photocharging rate in our photoelectrochemical system with TiO_2 and $K_2S_2O_8$.[17]

The water-in-salt LiTFSA electrolyte has much higher stability against oxidation compared to that of dilute aqueous solutions owing to its unique solvation structure,[21] and water oxidation was not suggested for $LiMn_{1.5}Fe_{0.5}O_4$. Thus, Co is responsible for extra amounts of the oxidation reaction. As shown in Fig. S17 (ESI†), *ex situ* X-ray absorption near-edge structure (XANES) analysis also revealed little change in the valence state of Mn after photocharging $LiMn_{1.5}Co_{0.5}O_4$. In contrast, an edge shift toward higher energy indicating Mn oxidation was clearly observed for $LiMn_{1.5}Fe_{0.5}O_4$ (Fig. S18, ESI†).

In summary, we successfully demonstrated the feasibility of photocharging $LiMn_2O_4$-based spinel-oxide materials, which are compositionally modified to improve the stability. We compared photoelectrochemical properties of $LiMn_{1.5}M_{0.5}O_4$ (M = Fe, Co, Ni, Zn) cathode materials and revealed that there are trade–off relationships between stability under illumination and capacity, depending on the amount of Mn^{3+} in the spinel-oxide materials. $LiMn_{1.5}Fe_{0.5}O_4$ has a good balance of them and, consequently, exhibited discharge capacities substantially higher than those of $LiMn_2O_4$. One of the great advantages of spinel materials is their high designability in the structure.[34,35] We hope that this work will provide fundamental guidelines for designing spinel-oxide cathode materials and promote the development of advanced PRBs.

This work was supported by JSPS KAKENHI (grant numbers 20K22460, 22K14499, 22H02265, 21H0164, 22KK0068) and by NIMS Joint Research Hub Program (QN3510). XRD analysis and SEM observation were carried out at the NIMS Battery Research Platform. We thank Dr F. Sakamoto for the technical help with ICP-OES at the Analytical Research Core for Advanced Materials, Institute for Materials Research, Tohoku University.

Conflicts of interest

There are no conflicts to declare.

Notes and references

1 A. D. Salunke, S. Chamola, A. Mathieson, B. D. Boruah, M. De Volder and S. Ahmad, *ACS Appl. Energy Mater.*, 2022, **5**, 7891–7912.
2 J. Lv, J. Xie, A. G. A. Mohamed, X. Zhang and Y. Wang, *Chem. Soc. Rev.*, 2022, **51**, 1511–1528.
3 A. G. Hodes, J. Manassen and D. Cahen, *Nature*, 1976, **261**, 403–404.
4 O. Nguyen, E. Courtin, F. Sauvage, N. Krins, C. Sanchez and C. Laberty-Robert, *J. Mater. Chem. A*, 2017, **5**, 5927–5933.
5 A. Paolella, C. Faure, G. Bertoni, S. Marras, A. Guerfi, A. Darwiche, P. Hovington, B. Commarieu, Z. Wang and M. Prato, *et al.*, *Nat. Commun.*, 2017, **8**, 14643.
6 T. Nomiyama, K. Sasabe, K. Sakamoto and Y. Horie, *Jpn. J. Appl. Phys.*, 2015, **54**, 071101.
7 W. Guo, X. Xue, S. Wang, C. Lin and Z. L. Wang, *Nano Lett.*, 2012, **12**, 2520–2523.
8 B.-M. Kim, M.-H. Lee, V. S. Dilimon, J. S. Kim, J. S. Nam, Y.-G. Cho, H. K. Noh, D.-H. Roh, T.-H. Kwon and H.-K. Song, *Energy Environ. Sci.*, 2020, **13**, 1473–1480.
9 M.-H. Lee, B.-M. Kim, Y. Lee, H.-G. Han, M. Cho, T.-H. Kwon and H.-K. Song, *ACS Energy Lett.*, 2021, **6**, 1198–1204.
10 S. Ahmad, C. George, D. J. Beesley, J. J. Baumberg and M. De Volder, *Nano Lett.*, 2018, **18**, 1856–1862.
11 B. D. Boruah, A. Mathieson, B. Wen, S. Feldmann, W. M. Dose and M. De Volder, *Energy Environ. Sci.*, 2020, **13**, 2414–2421.
12 B. D. Boruah and M. De Volder, *J. Mater. Chem. A*, 2021, **9**, 23199–23205.
13 X. Zhang, K. Su, A. G. A. Mohamed, C. Liu, Q. Sun, D. Yuan, Y. Wang, W. Xue and Y. Wang, *Energy Environ. Sci.*, 2022, **15**, 780–785.
14 N. Tewari, S. B. Shivarudraiah and J. E. Halpert, *Nano Lett.*, 2021, **21**, 5578–5585.
15 H. Liu, P. Wu, R. Wang, H. Meng, Y. Zhang, W. Bao and J. Li, *ACS Nano*, 2023, **17**, 1560–1569.
16 R. Zhang, Z. Chen, J. Ma, P. Zhang, M. Liu, X. Li, R. Zhao, J. Tang, Z. Ren and S. Li, *Chem. Commun.*, 2023, **59**, 2911–2914.
17 K. Shimokawa, S. Matsubara, A. Okamoto and T. Ichitsubo, *Chem. Commun.*, 2022, **58**, 9634–9637.
18 M. M. Thackeray, *Prog. Solid State Chem.*, 1997, **25**, 1–71.
19 A. Lee, M. Vörös, W. M. Dose, J. Niklas, O. Poluektov, R. D. Schaller, H. Iddir, V. A. Maroni, E. Lee, B. Ingram, L. A. Curtiss and C. S. Johnson, *Nat. Commun.*, 2019, **10**, 4946.
20 J. Lipton, Y. Ma, J. A. Röhr, J. Zhu, H. Wang, S. A. Maclean, C. S. Johnson and A. D. Taylor, *Cell Rep. Phys. Sci.*, 2022, **3**, 101051.
21 L. Suo, O. Borodin, T. Gao, M. Olguin, J. Ho, X. Fan, C. Luo, C. Wang and K. Xu, *Science*, 2015, **350**, 938–943.
22 L. Guohua, H. Ikuta, T. Uchida and M. Wakihara, *J. Electrochem. Soc.*, 1996, **143**, 178–182.
23 R. Bittihn, R. Herr and D. Hoge, *J. Power Sources*, 1993, **43**, 223–231.
24 R. J. Gummow, A. De Kock and M. M. Thackeray, *Solid State Ionics*, 1994, **69**, 59–67.
25 T. Ohzuku, S. Takeda and M. Iwanaga, *J. Power Sources*, 1999, **81–82**, 90–94.
26 A. Varma, A. S. Mukasyan, A. S. Rogachev and K. V. Manukyan, *Chem. Rev.*, 2016, **116**, 14493–14586.
27 K. Shimokawa, T. Atsumi, M. Harada, R. E. Ward, M. Nakayama, Y. Kumagai, F. Oba, N. L. Okamoto, K. Kanamura and T. Ichitsubo, *J. Mater. Chem. A*, 2019, **7**, 12225–12235.
28 K. Shimokawa, T. Atsumi, N. L. Okamoto, T. Kawaguchi, S. Imashuku, K. Wagatsuma, M. Nakayama, K. Kanamura and T. Ichitsubo, *Adv. Mater.*, 2021, **33**, 2007539.
29 W. Miran, W. Huang, X. Long, G. Imamura and A. Okamoto, *Patterns*, 2022, **3**, 100637.
30 Y. Ein-Eli, W. Wen and S. Mukerjee, *Electrochem. Solid-State Lett.*, 2005, **8**, A141–A144.
31 M. Kunduraciz and G. G. Amatucci, *J. Electrochem. Soc.*, 2006, **153**, A1345–A1352.
32 X. Deng and H. Tüysüz, *ACS Catal.*, 2014, **4**, 3701–3714.
33 M. Okazaki, Y. Wang, T. Yokoi and K. Maeda, *J. Phys. Chem. C*, 2019, **123**, 10429–10434.
34 K. Shimokawa, T. Hatakeyama, H. Li and T. Ichitsubo, *Curr. Opin. Electrochem.*, 2023, **38**, 101209.
35 K. Shimokawa and T. Ichitsubo, *Curr. Opin. Electrochem.*, 2020, **21**, 93–99.